

Magnetoencephalography with an atomic magnetometer

H. Xia, A. Ben-Amar Baranga, D. Hoffman, and M. V. Romalis^{a)}
Department of Physics, Princeton University, Princeton, New Jersey 08544

(Received 5 September 2006; accepted 5 October 2006; published online 21 November 2006)

The authors demonstrate detection and mapping of brain magnetic fields evoked by auditory stimulation with a noncryogenic magnetometer based on spin precession of potassium atoms in spin-exchange-relaxation-free regime. Optical readout using a photodiode array allows flexibility in detector placement while using common elements for most components of the multichannel system. Absence of a cryogenic dewar eliminates magnetic Johnson noise from radiation shields and allows the use of a compact magnetic shield with a high shielding factor. The magnetometer sensitivity is currently equal to $3.5 \text{ fT/Hz}^{1/2}$ at 10 Hz, similar to superconducting quantum interference device magnetoencephalography systems. © 2006 American Institute of Physics.
 [DOI: 10.1063/1.2392722]

Since the detection of magnetic fields generated by the brain with a low- T_c superconducting quantum interference device (SQUID) magnetometer,¹ magnetoencephalography (MEG) has developed into a powerful technique for functional brain imaging^{2,3} that is used both in basic science⁴ and clinical applications,⁵ while SQUID magnetometers cooled in LHe remained the only detectors with sufficient sensitivity to be used for MEG. Modern MEG systems contain several hundred sensors placed in a helmet-shaped LHe dewar⁶ and constitute the largest application of SQUIDs. Optically pumped alkali-metal magnetometers also have a long history⁷ but only recently achieved the sensitivity and spatial resolution competitive with low- T_c SQUIDs.⁸ Measurements of heart magnetic fields with an atomic magnetometer were demonstrated in Ref. 9 and further explored recently,¹⁰ but brain magnetic fields, which are 100 times weaker, are more challenging to detect.

The magnetometer is based on the measurement of electron Larmor spin precession in a vapor of potassium atoms. The atoms are spin polarized by a 0.5 W circularly polarized pump laser tuned to the D1 resonance at 770 nm and their precession in the magnetic field is detected by measuring the optical rotation of a 0.5 W probe laser beam detuned by approximately 0.2 nm from the resonance. The sensitivity of the magnetometer is determined by the density of K atoms and their spin-coherence time. At high density the spin-coherence time is usually limited by spin-exchange collisions between K atoms. However, relaxation due to spin-exchange collisions can be eliminated by operating the magnetometer near zero field, in the regime where the spin-exchange rate is much larger than the Larmor precession frequency.¹¹ Such spin-exchange-relaxation-free (SERF) magnetometer has achieved magnetic field sensitivity of $0.5 \text{ fT/Hz}^{1/2}$ with a 0.3 cm^3 active volume,⁸ surpassing the sensitivity of dc SQUID magnetometers. The fundamental sensitivity limit of a SERF magnetometer is on the order of $0.01 \text{ fT/Hz}^{1/2}$, allowing it to reach thermal magnetic noise of the human body, estimated to be $0.1 \text{ fT/Hz}^{1/2}$.³

The diagram of the human magnetoencephalography system is shown in Fig. 1. The core of the optical magnetometer is a $7.5 \times 7.5 \times 7.5 \text{ cm}^3$ Pyrex cell heated to $180 \text{ }^\circ\text{C}$ by

flowing hot air to obtain K vapor density of $3 \times 10^{13} \text{ cm}^{-3}$. It is substantially easier to maintain this elevated temperature compared to cryogenic LHe dewars since much larger power can be used for cell heating. The oven is constructed using only electrically insulating materials to avoid magnetic noise due to Johnson currents that usually limit magnetic field sensitivity in dewars. The surface of the oven facing the subject is maintained at room temperature by flowing water through a thin cooling pad and is insulated from the cell by a 7 mm thick microporous ceramic insulation. Pump and probe laser beams pass through insulating double-walled glass cells with a dielectric coating that is highly reflective for thermal radiation in the far infrared but has low reflectivity at 770 nm.¹²

The magnetometer is placed in a three layer μ -metal cylindrical shield with an inner diameter of 1 m and length of 2.6 m. The transverse shielding factor is equal to 7×10^3 and longitudinal shielding factor is 10^3 , significantly larger than for typical magnetically shielded rooms used with

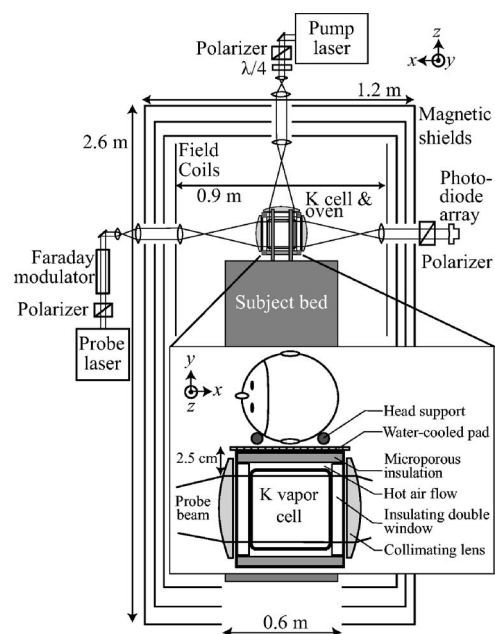


FIG. 1. Experimental setup for optical magnetoencephalography system. The total distance between the probe beam and the room-temperature surface is 2.5 cm, limited in part by optical imperfections of the K cell.

^{a)}Electronic mail: romalis@princeton.edu

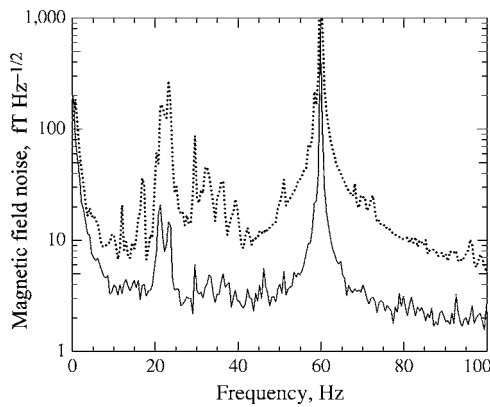


FIG. 2. Magnetic noise spectrum of the magnetometer obtained with six-channel photodetector. Dotted line: single channel noise. Solid line: intrinsic magnetometer noise determined from the noise in the difference between two adjacent channels separated by 5 mm.

SQUID MEG systems. Subject access is provided through a 0.6 m diameter hole that remains open during measurements, having a negligible effect on the shielding factor due to exponential attenuation of field penetration into a cylindrical shield through an open end.^{13,14} Absence of a large cryogenic dewar allows the use of magnetic shields with a much smaller characteristic size L than typical for shielded rooms, which improves the shielding factor that scales as $1/L$, while reducing the weight and cost of the shields that scale as L^2 . The inside diameter of the magnetic shields is still larger than the bore of typical magnetic resonance imaging magnets, ensuring adequate subject comfort.

The optical rotation of the probe beam is measured using a polarization modulation technique. The beam passes through a Faraday rotator that modulates the angle of its linear polarization at 3 kHz. After the cell, the polarization of the beam is analyzed with a crossed linear polarizer. The photodiode signal is digitized and the optical rotation is determined from the first harmonic of the modulation frequency with a digital lock-in amplifier. Magnetic field mapping is performed by imaging the probe beam onto a multichannel photodetector. About 1 atm of He buffer gas is added to the cell to limit the diffusion of K atoms between regions corresponding to different detector channels. Brain signals are recorded with a six element linear photodetector array or a two-dimensional (2D) 16×16 element array. For the 256 element photodiode array the lock-in demodulation is implemented using field programmable gate array on a custom data acquisition board.¹⁵ Optical mapping allows flexibility in imaging of the cell volume onto the detector array while using common elements for most components of the multichannel system, and thus reducing system cost.

Residual magnetic fields inside the shields are on the order of $10 \mu\text{G}$ and need to be zeroed for optimal operation of the SERF magnetometer. The fields are canceled by a system of 18 computer-controlled coils inside the shields. Maps of the magnetic fields created by each coil are used to determine linear combinations of coil currents that generate uniform fields and linear gradients. All three magnetic field components are measured independently by applying appropriate field modulations¹⁶ and zeroed to within $0.3 \mu\text{G}$ every few hours. The magnetometer is calibrated by applying known magnetic fields and the spatial mapping from the

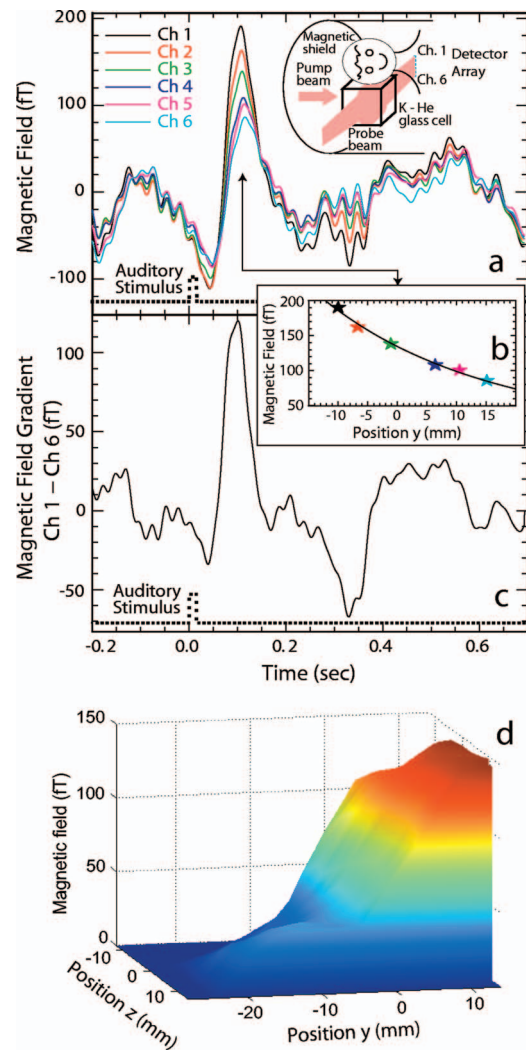


FIG. 3. (Color) Auditory evoked magnetic fields obtained with atomic magnetometer after averaging 600 stimuli presentations. Magnetic fields recorded with a six-channel linear photodetector [panel (a)] and magnetic field gradient determined from the difference between the two outermost channels [panel (c)] as a function of time. The magnetic field background fluctuations [seen, for example, before the auditory stimulus in panel (a)] are significantly reduced in the gradient measurement. The spatial dependence of the magnetic field at 100 ms after the stimulus is shown in panel (b) with a dipolar field fit. 2D spatial distribution of magnetic fields recorded with 16×16 photodiode array at 100 ms after the stimulus is shown in panel (d).

magnetometer cell to each photodiode position is determined by applying a uniform field gradient.

The noise spectrum of the magnetometer measured with the six element linear photodetector array is shown in Fig. 2. Single channel noise is dominated by leakage of external magnetic field fluctuations and mechanical vibrations. The intrinsic magnetometer noise, determined by dividing the noise in the difference between two adjacent channels by a factor of $\sqrt{2}$, is limited by optical rotation measurement noise. The noise level of the magnetometer for frequencies higher than 10 Hz is equal to $3.5 \text{ fT/Hz}^{1/2}$ similar to commercial SQUID MEG systems.⁶ The $1/f$ noise is likely due to laser fluctuations caused by air convection and is presently somewhat worse than in SQUID systems. The frequency response of the magnetometer is given by a first-order low-pass filter with a width of 25 Hz, containing most of the frequency spectrum of brain magnetic fields.³

Evoked magnetic fields from human subjects were measured by applying auditory stimuli to the subject's ear oppo-

site to the magnetometer cell with a pneumatic earphone. Each stimulus consists of 16 square pulses with a period of 1 ms and duty cycle of 20%.¹⁷ The interval between each train of clicks is varied randomly between 0.9 and 1.7 s to avoid subject adaptation. In analysis, the signal is first filtered with a 0.9–40 Hz bandpass fast Fourier transform (FFT) filter and three FFT notch filters (19–25, 28–30 and 34–36 Hz) are used to remove narrow line interference without distorting the shape of the signals. Signals within a window from 0.2 s before to 0.7 s after the onset of each stimulus are averaged for 600 presentations of the stimulus. For 2D data, the field profile is smoothed with a Gaussian filter with a width of 1 pixel. Signals from six subjects have been recorded with similar results, following a protocol approved by the Institutional Review Board. All subjects were at least 18 years of age and signed a consent form.

The radial magnetic field (y direction in Fig. 1) is shown in Fig. 3(a) for six channels distributed radially away from the subject's head with a spacing of approximately 5 mm. In Fig. 3(b) we plot the gradient of the magnetic field, determined from the difference between the two outermost channels, showing significant cancelation of common-mode magnetic field drift that is seen in the individual channel field measurements. The magnetic fields and gradients clearly show the N100m peak commonly observed 100 ms after auditory stimuli.³ There is also evidence in the magnetic field gradient for a P300m peak at 300 ms that may be due to random onset time of the stimuli.¹⁸ Figure 3(c) shows the spatial distribution of the magnetic field at the N100m peak as a function of the distance away from the head with a fit to a dipole field profile. Finally, in Fig. 3(d) we show the spatial distribution of magnetic fields recorded with the 2D photodiode array at the N100m peak of brain activity. The spatial profile of magnetic fields can be used to localize the region of brain activation, although the spatial extent of field measurements is currently less than optimal due to optical distortions near the edge of the cell.

In conclusion, we have demonstrated the detection and mapping of brain magnetic field by a noncryogenic magne-

tometer. Future improvements include reduction of low frequency magnetic noise and exploration of various configurations of pump and probe beams to measure different components of the magnetic field and different mapping geometries. For example, by selectively illuminating only a part of the cell with the pump beam it is possible to obtain a three-dimensional map of the magnetic field. It is also possible to obtain nearly full head coverage using four glass cells. Fiber-optic-coupled sensors would offer additional flexibility in detector placement. The flexibility and low cost of optical field mapping, as well as its potentially higher sensitivity, should open new applications for functional brain imaging.

The authors would like to thank V. van Wassenhove, J. Haxby, and K. Kim for useful discussions. This work was supported by the NIH.

¹D. Cohen, *Science* **175**, 664 (1972).

²C. Del Gratta, V. Pizzella, F. Tecchio, and G. L. Romani, *Rep. Prog. Phys.* **64**, 1759 (2001).

³M. Hämäläinen, R. Hari, R. J. Ilmoniemi, J. Knuutila, and O. V. Lounasmaa, *Rev. Mod. Phys.* **65**, 413 (1993).

⁴A. D. Patel and E. Balaban, *Nature (London)* **404**, 80 (2000).

⁵A. C. Papanicolaou, E. M. Castillo, R. Billingsley-Marshall, E. Patariaia, and P. G. Simos, *Int. Rev. Neurobiol.* **68**, 223 (2005).

⁶For example, Elekta Neuromag® at www.elekta.com

⁷A. L. Bloom, *Appl. Opt.* **1**, 61 (1962).

⁸I. K. Kominis, T. W. Kornack, J. C. Allred, and M. V. Romalis, *Nature (London)* **422**, 596 (2003).

⁹M. N. Livanov, A. N. Kozlov, A. V. Korinevskii, V. P. Markin, S. E. Sinelnikova, and I. A. Kholodov, *Dokl. Akad. Nauk SSSR* **238**, 253 (1978).

¹⁰G. Bison, R. Wynands, and A. Weis, *Opt. Express* **11**, 904 (2003).

¹¹W. Happer and H. Tang, *Phys. Rev. Lett.* **31**, 273 (1973).

¹²Esco Products, Oak Ridge, New Jersey.

¹³A. J. Mager, *IEEE Trans. Magn.* **6**, 67 (1970).

¹⁴E. Paperno, I. Sasada, and K. Tashiro, *IEEE Trans. Magn.* **38**, 3324 (2002).

¹⁵D-TACQ Solutions Ltd., East Kilbride, Scotland, U.K.

¹⁶S. J. Seltzer and M. V. Romalis, *Appl. Phys. Lett.* **85**, 4804 (2004).

¹⁷S. Nakagawa, S. Ueno, and T. Imada, *J. Appl. Phys.* **85**, 5708 (1999).

¹⁸D. E. J. Linden, *Neuroscientist* **11**, 563 (2005).